PNAS RESEARCH ARTICLE | BIOCHEMISTRY OPEN ACCESS

Phosphorylation of RXRα mediates the effect of JNK to suppress hepatic FGF21 expression and promote metabolic syndrome

Santiago Vernia[a,b,1,2], Alexandra Lee[c,1], Norman J. Kennedy[c,1], Myoung Sook Han[c], Marta Isasa[d,3], Julie Cavanagh-Kyros[c], Armanda Roy[c], Aafreen Syed[c], Shanzah Chaudhry[c], Yvonne J. K. Edwards[c,4], Steven P. Gygi[d], Guangping Gao[e], and Roger J. Davis[c,2]

Contributed by Roger Davis; received June 16, 2022; accepted September 8, 2022; reviewed by J. Silvio Gutkind and Robert E. Lewis

The cJun NH_2-terminal kinase (JNK) signaling pathway in the liver promotes systemic changes in metabolism by regulating peroxisome proliferator-activated receptor α (PPARα)-dependent expression of the hepatokine fibroblast growth factor 21 (FGF21). Hepatocyte-specific gene ablation studies demonstrated that the *Mapk9* gene (encoding JNK2) plays a key mechanistic role. Mutually exclusive inclusion of exons 7a and 7b yields expression of the isoforms JNK2α and JNK2β. Here we demonstrate that *Fgf21* gene expression and metabolic regulation are primarily regulated by the JNK2α isoform. To identify relevant substrates of JNK2α, we performed a quantitative phosphoproteomic study of livers isolated from control mice, mice with JNK deficiency in hepatocytes, and mice that express only JNK2α or JNK2β in hepatocytes. We identified the JNK substrate retinoid X receptor α (RXRα) as a protein that exhibited JNK2α-promoted phosphorylation in vivo. RXRα functions as a heterodimeric partner of PPARα and may therefore mediate the effects of JNK2α signaling on *Fgf21* expression. To test this hypothesis, we established mice with hepatocyte-specific expression of wild-type or mutated RXRα proteins. We found that the RXRα phosphorylation site Ser^{260} was required for suppression of *Fgf21* gene expression. Collectively, these data establish a JNK-mediated signaling pathway that regulates hepatic *Fgf21* expression.

high-fat diet | insulin resistance | JNK | RXRα | FGF21

Significance

The cJUN NH_2-terminal kinase (JNK) signaling pathway is activated by metabolic stress and plays a key role during the development of metabolic syndrome. JNK2 acts in the liver by suppressing the expression of the hepatokine fibroblast growth factor 21 (FGF21). We show that the alternatively spliced JNK2α isoform mediates the effects of metabolic stress. Quantitative phosphoproteomics analysis and functional testing using genetic complementation analysis demonstrated that JNK2α-mediated phosphorylation of retinoid X receptor α (RXRα) inhibits FGF21 expression. These observations define a JNK/RXRα/FGF21 signaling axis that contributes to obesity-associated metabolic syndrome.

The hepatic cJUN NH_2-terminal kinase (JNK) signaling pathway is activated by nutritional stress, including the consumption of a high-fat diet (HFD) (1). Hepatocyte-specific ablation of the *Mapk8* gene (encoding JNK1) causes increased hepatic steatosis in HFD-fed mice (2). In contrast, hepatocyte-specific ablation of *Mapk9* (encoding JNK2) or *Mapk8* plus *Mapk9* causes systemic improvement of insulin resistance, hyperglycemia, and hyperlipidemia in HFD-fed mice (3). These different roles of JNK1 and JNK2 reflect actions on the nuclear hormone receptor NR1C1 (also known as the peroxisome proliferator-activated receptor α [PPARα]) that is suppressed in response to JNK signaling in HFD-fed wild-type mice (3). Increased hepatic PPARα-mediated gene expression promotes fatty acid oxidation and increased expression of the hepatokine fibroblast growth factor 21 (FGF21) (4, 5) in response to JNK2 deficiency, but these actions are suppressed by JNK1 deficiency (3). These PPARα-dependent changes in fatty acid oxidation and FGF21 expression provide a mechanism for systemic regulation of insulin resistance caused by JNK signaling in hepatocytes. Indeed, it is established that JNK2 acts to suppress hepatic *Fgf21* gene expression and promotes systemic insulin resistance by reducing the amount of FGF21 circulating in the blood (3, 6).

The hepatokine FGF21 responds to nutritional stress and is secreted as an endocrine hormone in the blood primarily by hepatocytes (7–10). Circulating FGF21 acts on adipocytes by increasing PGC1α and thermogenic gene expression (11), increasing NR1C3 (also known as PPARγ) activity and insulin sensitization (12), and increasing adipokine expression (13–16). FGF21 also targets the central nervous system (17) and regulates behavior (18), food choice preference (19–22), and water consumption (23) and increases sympathetic outflow (18, 24). FGF21 therefore plays a key role in the response to nutritional stress.

The mechanism that mediates the regulation of hepatic *Fgf21* gene expression by JNK is unclear. Nevertheless, it is known that JNK2 inhibits PPARα transcriptional activity in the liver (3), that PPARα increases hepatic *Fgf21* gene expression (4, 5), and that PPARα is required for JNK2-regulated *Fgf21* gene expression (3). Moreover, it is established that PPARα functions within heterodimeric complexes with the partner protein NR2B1 (also known as retinoid X receptor α [RXRα]) (25).

Author contributions: S.V. and R.J.D. designed research; S.V., A.L., N.J.K., M.S.H., M.I., J.C.-K., A.R., A.S., and S.C. performed research; S.V., A.L., N.J.K., M.S.H., M.I., Y.J.K.E., S.P.G., G.G., and R.J.D. analyzed data; and S.V., A.L., N.J.K., M.S.H., M.I., Y.J.K.E., S.P.G., G.G., and R.J.D. wrote the paper.

Reviewers: J.S.G., University of California San Diego Medical Center; and R.E.L., University of Nebraska Medical Center.

The authors declare no competing interest.

[1]S.V., A.L., and N.J.K. contributed equally to this work.

[2]To whom correspondence may be addressed. Email: Santiago.Vernia@lms.mrc.ac.uk or Roger.Davis@umassmed.edu.

[3]Present address: Odyssey Therapeutics, Cambridge, MA 02142.

[4]Present address: Department of Biochemistry and Molecular Genetics, University of Alabama at Birmingham, Birmingham, AL 35294.

This article contains supporting information online at http://www.pnas.org/lookup/suppl/doi:10.1073/pnas.2210434119/-/DCSupplemental.

Published October 25, 2022.

We report that JNK-mediated repression of *Fgf21* expression is selectively mediated by the alternatively spliced isoform JNK2α. Comparative phosphoproteomics analysis identified JNK2α-dependent phosphorylation of RXRα. Mutational analysis of RXRα demonstrated that the JNK phosphorylation site Ser^{260} was required for JNK-mediated repression of *Fgf21* expression. Collectively, these observations identify a mechanism that accounts for JNK-regulated *Fgf21* gene expression in the liver and the development of metabolic syndrome.

Results

Hepatic JNK2α Plays a Major Role in the Regulation of Glycemia. It is established that JNK2 in the liver plays a key role in the regulation of glycemia (3). However, the relevant JNK2 isoform has not been identified. Alternative splicing of *Mapk9* pre-messenger RNA (mRNA) results in the mutually exclusive inclusion of exon 7a or exon 7b and expression of the JNK2α and JNK2β isoforms (26, 27). These JNK isoforms differ in their protein kinase activity, and both isoforms are expressed in the liver of wild-type mice (26, 27). Thus, the canonical substrate JUN is preferentially phosphorylated by JNK2α (26, 27). Whether JNK2β functions as a low-activity form of JNK2α or whether JNK2β represents an independent noncanonical JNK signaling pathway is unclear.

To test the role of the JNK2α and JNK2β isoforms, we used complementation assays using mice with hepatocyte-specific deficiency of JNK (*Alb-Cre*$^{-/+}$ *Mapk8*$^{loxP/loxP}$ *Mapk9*$^{loxP/loxP}$). Control studies were performed by examining the effect of adeno-associated vectors serotype 8 (AAV8)-mediated expression of JNK2α and JNK2β on JUN phosphorylation. These studies demonstrated that, as expected, JUN phosphorylation in the liver was preferentially restored by JNK2α (Fig. 1*A*). This analysis confirmed that the JNK2α and JNK2β isoforms may serve different functions in vivo.

A major function of JNK signaling in the liver is the suppression of PPARα-mediated expression of the hepatokine FGF21 (3, 6). Indeed, in vitro studies using fibrate-stimulated primary hepatocytes demonstrated that PPARα-mediated gene expression was suppressed by JNK2 (*SI Appendix*, Fig. S1). Moreover, PPARα-mediated gene expression was more potently suppressed by JNK2α than JNK2β (*SI Appendix*, Fig. S1). We therefore examined the effect of expression of JNK2α and JNK2β in hepatocytes on the circulating concentration of FGF21 in the blood. This analysis demonstrated that the blood concentration of FGF21 was lower in mice with hepatic JNK2α than in mice with hepatic JNK2β (Fig. 1*B*). These data demonstrate that JNK2α more potently represses hepatic FGF21 expression than does JNK2β in vivo.

Tissue-specific gene ablation studies demonstrate that the regulation of glycemia by hepatic JNK is mediated by FGF21 (3, 6). Since JNK2α selectively regulates FGF21 expression (Fig. 1*B*), we anticipated that JNK2α may play a larger role than JNK2β in the regulation of glycemia. To test this hypothesis, we examined the blood glucose concentration in mice expressing JNK2α or JNK2β in hepatocytes. We found that JNK2α caused increased fasting hyperglycemia in HFD-fed mice compared with JNK2β (Fig. 1*C*). Moreover, JNK2α expression in hepatocytes caused increased intolerance to glucose (Fig. 1*D*) and pyruvate (Fig. 1*E*) compared with JNK2β.

Collectively, these data demonstrate that the JNK2α isoform plays a major role in the liver and that the function of hepatic JNK2β is unclear. Molecular mechanisms of signaling by hepatic JNK2α and JNK2β remain to be established.

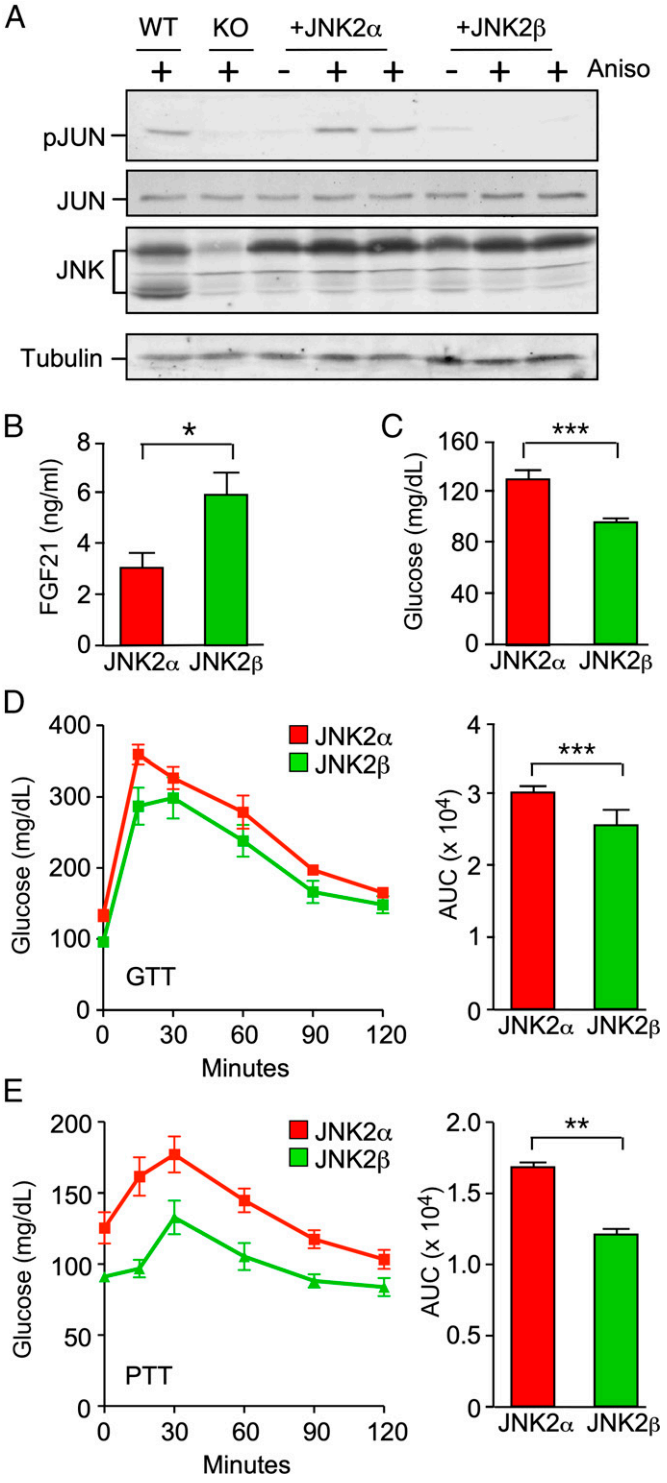

Fig. 1. Complementation analysis demonstrates a selective role for hepatic JNK2α in the regulation of glycemia. (*A*) Primary hepatocytes prepared from wild-type (WT) mice (*Alb-Cre*$^{-/+}$ *Mapk8*$^{+/+}$ *Mapk9*$^{+/+}$), knockout (KO) mice with hepatocyte-specific JNK1 plus JNK2 KO (*Alb-Cre*$^{-/+}$ *Mapk8*$^{loxP/loxP}$ *Mapk9*$^{loxP/loxP}$), and KO mice complemented with AAV-mediated expression of JNK2α or JNK2β were treated with 1 μg/mL anisomycin (Aniso) (15 min). Lysates were examined by immunoblot analysis by probing with antibodies to $pSer^{63}$ JUN (pJUN), JUN, JNK, and α-tubulin. (*B* and *C*) Blood FGF21 and glucose concentration in HFD-fed mice (16 wk) expressing JNK2α or JNK2β in hepatocytes was measured (mean ± SEM; $^{*}P < 0.05$, $^{***}P < 0.001$; $n = 6$~8). (*D* and *E*) GTTs and PTTs on HFD-fed mice (16 wk) expressing JNK2α or JNK2β in hepatocytes were performed and the area under the curve (AUC) was measured (mean ± SEM; $^{**}P < 0.01$, $^{***}P < 0.001$; $n = 6$~8).

Phosphoproteomics Analysis Identifies RXRα as a JNK2α Substrate. The signaling function of JNK is most likely mediated by the phosphorylation of a protein substrate. We anticipated that

this substrate would not be phosphorylated in the liver of mice with hepatic JNK deficiency. Moreover, the different substrate specificities of JNK2α and JNK2β (26, 27) indicate that complementation assays may lead to the identification of JNK2 isoform-selective substrates. We therefore performed global phosphoproteomic analysis on the liver of control mice and JNK-deficient mice. The mice were fed a HFD to activate the hepatic JNK signaling pathway. Quantitative mass spectroscopy of multiplexed samples labeled with isobaric tags for relative and absolute quantitation (iTRAQ) led to the identification of 8,955 phosphopeptides (Fig. 2*A* and *SI Appendix*, Dataset S1). To identify those phosphorylation sites that may correspond to JNK substrates, we examined the subset of phosphorylation sites that conform to the consensus sequences pSer-Pro and pThr-Pro (28). We found phosphorylation sites that were down-regulated in JNK-deficient liver compared with control liver. These phosphorylation sites correspond to potential JNK substrate sites. To identify those phosphorylation sites that may be preferentially regulated by JNK2α, we compared hepatic phosphorylation in mice with JNK deficiency complemented with JNK2α or JNK2β in hepatocytes (Fig. 2*B*). This analysis identified proteins that were selectively phosphorylated on consensus sites in JNK2α-complemented liver (cluster 2, including ABLIM3, AFF4, ALAS1, ARHGAP2, CD2AP, CLASRP, GAREM, IRS2, JUN, MACF1, MAP4, MAP7D1, MEF2D, MTSS1, NUCKS1, PIK3C2A, PLEKHA5, PPFIA1, RBBP6, RRBP1, RXRα, SELENBP1, SIPA1L1, SPTBN1, SQSTM1, SRPK1, SRRM1, SYNPO, TACC2, TRIM25, and ZNF768) and JNK2β-complemented liver (cluster 1, including ABCF1, CARD6, EIF4EBP, GAS2, MTUS1, OSBPL, PLEKHA6, SRRM1, and SRRM2). Phosphorylation of one or more of these proteins may contribute to selective signaling by the hepatic isoforms JNK2α and JNK2β.

The potential JNK2α substrates identified by phosphoproteomics included the nuclear hormone receptor RXRα that functions as a heterodimeric partner of PPARα. This finding suggested that RXRα phosphorylation may mediate the effects of JNK2α on the PPARα/FGF21 signaling axis. Indeed, in vitro studies have established that RXRα is a JNK substrate (29). We performed immunoblot analysis of hepatocytes isolated from control mice (*Alb-Cre*$^{-/+}$ *Mapk8*$^{+/+}$ *Mapk9*$^{+/+}$) and mice with compound deficiency of JNK1 plus JNK2 in hepatocytes (*Alb-Cre*$^{-/+}$ *Mapk8*$^{loxP/loxP}$ *Mapk9*$^{loxP/loxP}$) by probing with an antibody to phospho-RXRα. We found that JNK deficiency prevented RXRα phosphorylation (Fig. 2*C*). Moreover, complementation analysis of JNK-deficient mice demonstrated that RXRα phosphorylation was restored more efficiently by JNK2α than JNK2β (Fig. 2*C*). These data demonstrate JNK2α regulates hepatic RXRα phosphorylation.

JNK Phosphorylation of Hepatic RXRα Regulates PPARα Signaling. To test the role of JNK-mediated RXRα phosphorylation, we employed a genetic complementation assay using mice with conditional expression of the *Rxrα* gene. We employed *SA-Cre*$^{ERT2+/-}$ mice with insertion of an *IRES-Cre*^{ERT2} cassette in the 3′ untranslated region of the serum albumin gene (30) to establish *SA-Cre*$^{ERT2+/-}$ *Rxrα*$^{loxP/loxP}$ mice with conditional RXRα expression in hepatocytes and control *SA-Cre*$^{ERT2+/-}$ mice. Treatment of *SA-Cre*$^{ERT2+/-}$ *Rxrα*$^{loxP/loxP}$ mice with tamoxifen caused hepatic *Rxrα* gene ablation and loss of hepatic *Rxrα* mRNA and murine RXRα protein expression (Fig. 3 *A* and *B*). Control studies demonstrated no compensatory changes in the expression of *Rxrβ* and *Rxrγ* mRNA following *Rxrα* gene ablation (*SI Appendix*, Fig. S2).

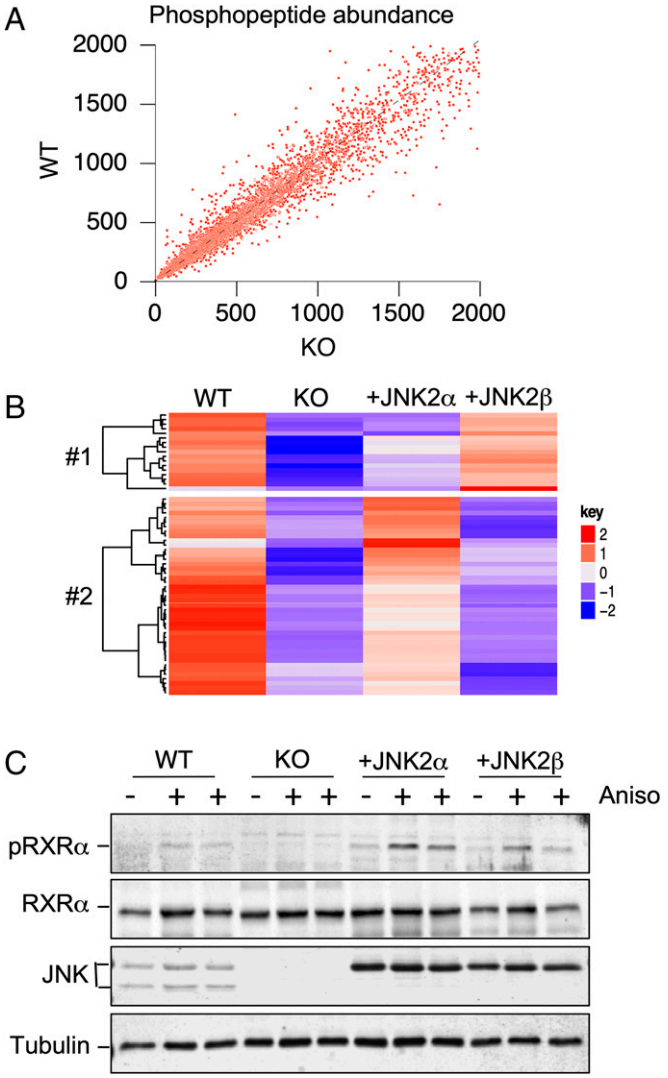

Fig. 2. Phosphoproteomics analysis identifies JNK-dependent phosphorylation of RXRα. (*A*) Quantitative mass spectroscopy of multiplexed samples labeled with iTRAQ tags identified 8,955 phosphopeptides. The abundance of detected phosphopeptides in the liver of HFD-fed (16 wk) mice was examined. Data obtained from WT and hepatocyte-specific JNK1 plus JNK2 KO mice are presented. (*B*) Phosphorylation sites that conform to the MAPK consensus sequence (Ser-Pro and Thr-Pro) that are phosphorylated in WT liver and exhibit decreased phosphorylation in hepatocyte-specific JNK1 plus JNK2 KO liver that is partially complemented by AAV8-mediated expression of JNK2α or JNK2β are presented as a heatmap. (*C*) Primary hepatocytes were treated with 1 μg/mL anisomycin (Aniso, 15 min). Lysates were probed using antibodies to pSer^{22} RXRα (pRXRα), RXRα, JNK, and α-tubulin.

We performed studies using tail vein administration of an AAV8 vector that expresses human RXRα (hRXRα) in hepatocytes of 7-wk-old mice. These mice were treated with tamoxifen at age 8 wk to ablate the endogenous murine *Rxrα* gene in hepatocytes. TaqMan assays demonstrated loss of murine *Rxra* mRNA and expression of human *Rxra* mRNA (Fig. 3*A*). To test the role of RXRα phosphorylation, we compared mice expressing hRXRα and mice expressing phosphorylation-defective hRXRα. The phosphorylation sites Ser^{22} and Ser^{265} on murine RXRα were identified by phosphoproteomics analysis of mouse liver (*SI Appendix*, Dataset S1). These phosphorylation sites correspond to Ser^{21} and Ser^{260} on hRXRα.

Our initial studies focused on mutation of Ser^{21} by replacing this residue with a nonphosphorylated amino acid (Ala) or with a potentially phosphomimetic residue (Asp). No difference in fasting blood FGF21 and glucose concentration was detected between mice expressing wild-type hRXRα and Ser21Ala hRXRα

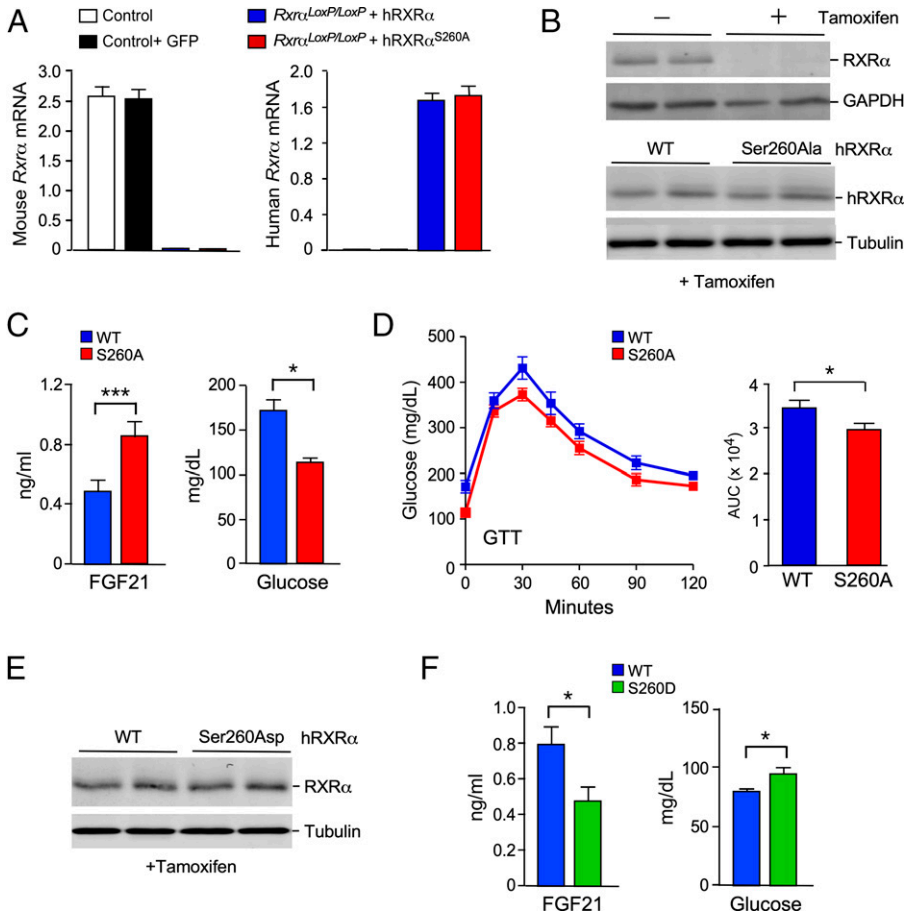

Fig. 3. Hepatic hRXRα phosphorylation on Ser^{260} increases FGF21 signaling. (*A*) Control *SA-Cre*^{ERT2} mice and *SA-Cre*^{ERT2} *Rxra*$^{loxP/loxP}$ mice (age 7 wk) were transduced with AAV8 viruses expressing green fluorescent protein (GFP), hRXRα, or Ser260Ala-hRXRα. The mice were treated without or with tamoxifen at age 8 wk, fed a HFD starting at age 10 wk, and euthanized at age 18 wk. Reverse transcriptase quantitative PCR (RT-qPCR) assays of murine liver to detected mouse and human *Rxra* mRNA are presented (mean ± SEM; n = 8~10). (*B*) Lysates of murine liver were examined by immunoblot analysis by probing with antibodies to RXRα, glyceraldehyde-3-phosphate dehydrogenase (GAPDH), and α-tubulin. (*C*) Fasting blood FGF21 and glucose concentration in HFD-fed mice expressing hRXRα or Ser260Ala hRXRα in hepatocytes was measured (mean ± SEM; *P < 0.05, ***P < 0.001; n = 9~10). (*D*) GTTs on HFD-fed mice expressing hRXRα or Ser260Ala hRXRα in hepatocytes were performed and the area under the curve (AUC) was measured (mean ± SEM; *P < 0.05; n = 7~10). (*E*) CD-fed mice expressing WT hRXRα or Ser260Asp hRXRα were euthanized at age 18 wk. Immunoblot analysis of liver extracts was performed by probing with antibodies to RXRα and α-tubulin. (*F*) Fasting blood FGF21 and glucose concentration in CD-fed mice expressing hRXRα or Ser260Asp hRXRα in hepatocytes was measured (mean ± SEM; *P < 0.05; n = 9).

(*SI Appendix*, Fig. S3 *A* and *B*) or Ser21Asp hRXRα (*SI Appendix*, Fig. S3 *D* and *E*) in hepatocytes. Similarly, mutation of Ser^{21} caused no change in glucose tolerance (*SI Appendix*, Fig. S3 *C* and *F*). This analysis indicates that Ser^{21} may not be a site of regulatory phosphorylation of hRXRα in the liver.

Our subsequent studies focused on the hRXRα phosphorylation site Ser^{260}. Similar levels of expression of wild-type hRXRα and Ser260Ala hRXRα were detected in AAV8-transduced *SA-Cre*$^{ERT2+/-}$ *Rxrα*$^{loxP/loxP}$ mice (Fig. 3*B*). We found that fasting hyperglycemia was reduced in HFD-fed mice expressing Ser260Ala hRXRα in hepatocytes compared with mice expressing wild-type hRXRα (Fig. 3*C*). The HFD-fed Ser260Ala hRXRα mice also exhibited reduced intolerance to glucose compared with HFD-fed wild-type RXRα mice (Fig. 3*D*). These differences were associated with an increased circulating concentration of FGF21 in mice with Ser260Ala hRXRα in hepatocytes compared with mice expressing wild-type RXRα (Fig. 3*C*). These data indicate that the phosphorylation of RXRα by JNK on Ser^{260} may inhibit RXRα function to promote *Fgf21* gene expression.

To test whether hRXRα phosphorylation at Ser^{260} inhibits function, we examined the effect of replacement of this phosphorylation site with a potentially phosphomimetic residue (Asp). Immunoblot analysis demonstrated that the wild-type hRXRα and Ser260Asp hRXRα proteins were expressed at similar levels in the liver (Fig. 3*E*). The fasting blood glucose concentration in chow diet (CD)-fed mice expressing Ser260Asp hRXRα in hepatocytes was increased compared with mice expressing wild-type hRXRα (Fig. 3*F*). Moreover, expression of Ser260Asp hRXRα in hepatocytes caused a reduction in the circulating concentration of FGF21 in fasted CD-fed mice compared with mice expressing wild-type hRXRα (Fig. 3*F*). These data confirm that hRXRα phosphorylation on Ser^{260} may suppress hepatic *Fgf21* gene expression.

JNK Causes Redistribution of RXRα from the Nucleus to the Cytoplasm. Phosphorylation is implicated as a regulatory mechanism that controls RXRα function. For example, phosphorylation may regulate RXRα degradation (31–33) and the interaction of RXRα with nuclear hormone receptors (34), the MED1 component of the mediator complex (35), the coactivator SRC-1 (36), and the corepressor RIP140 (35). These changes in RXRα function may be a secondary consequence of a change in subcellular localization (31). Indeed, it is established that RXRα cycles between the nucleus and the cytoplasm because of the presence of both a nuclear localization sequence and a CRM1-dependent

nuclear export sequence in RXRα (37, 38). Nucleocytoplasmic cycling of RXRα may regulate the subcellular localization of heterodimeric nuclear hormone receptor partners, including NR1l1 and NR4A1 (37, 38).

To examine whether this redistribution of RXRα from the nucleus to the cytoplasm is physiologically relevant, we prepared frozen hepatic sections from control CD-fed mice or mice fed a Western diet (WD) that causes metabolic stress-induced JNK activation. Immunoblot analysis demonstrated that the hepatic expression of RXRα and PPARα in CD-fed and WD-fed mice was similar (*SI Appendix*, Fig. S4). Immunofluorescence analysis of liver sections of CD-fed mice demonstrated that RXRα was primarily localized to the nucleus (Fig. 4*A*). In contrast, studies of WD-fed mice demonstrated that RXRα was primarily localized to the cytoplasm (Fig. 4*A*). This relocalization of RXRα to the cytoplasm was suppressed in *Alb-Cre*$^{-/+}$ *Mapk8*$^{loxP/loxP}$ *Mapk9*$^{loxP/loxP}$ mice with JNK deficiency in hepatocytes (Fig. 4*B*). Collectively, these data confirm that activated JNK promotes the redistribution of RXRα from the nucleus to the cytoplasm in response to hepatic metabolic stress (Fig. 4*C*). This JNK-promoted relocalization of RXRα to the cytoplasm may contribute to JNK-mediated repression of PPARα-dependent *Fgf21* gene expression.

Discussion

The activation of JNK in the liver promotes systemic insulin resistance that is mediated by inhibition of the heterodimeric nuclear hormone receptor RXRα/PPARα that results in reduced expression of the hepatokine FGF21 (3, 6). This inhibition is associated with decreased RXRα/PPARα DNA binding detected by chromatin immunoprecipitation assays (3). Here we demonstrate that the mechanism of inhibition may be mediated, in part, by phosphorylation of hRXRα on Ser^{260} (murine RXRα on Ser^{265}) by JNK2α and relocalization of the transcription factor from the nucleus to the cytoplasm.

It is established that RXRα is phosphorylated on several sites by casein kinase 1 (39), MAP kinase kinase 4 (40), mitogen-activated protein kinases (29, 33, 41), glycogen synthase kinase 3 (42–44), and protein kinase C (45). The hRXRα phosphorylation sites Ser^{21} and Ser^{260} (Ser^{22} and Ser^{265} in

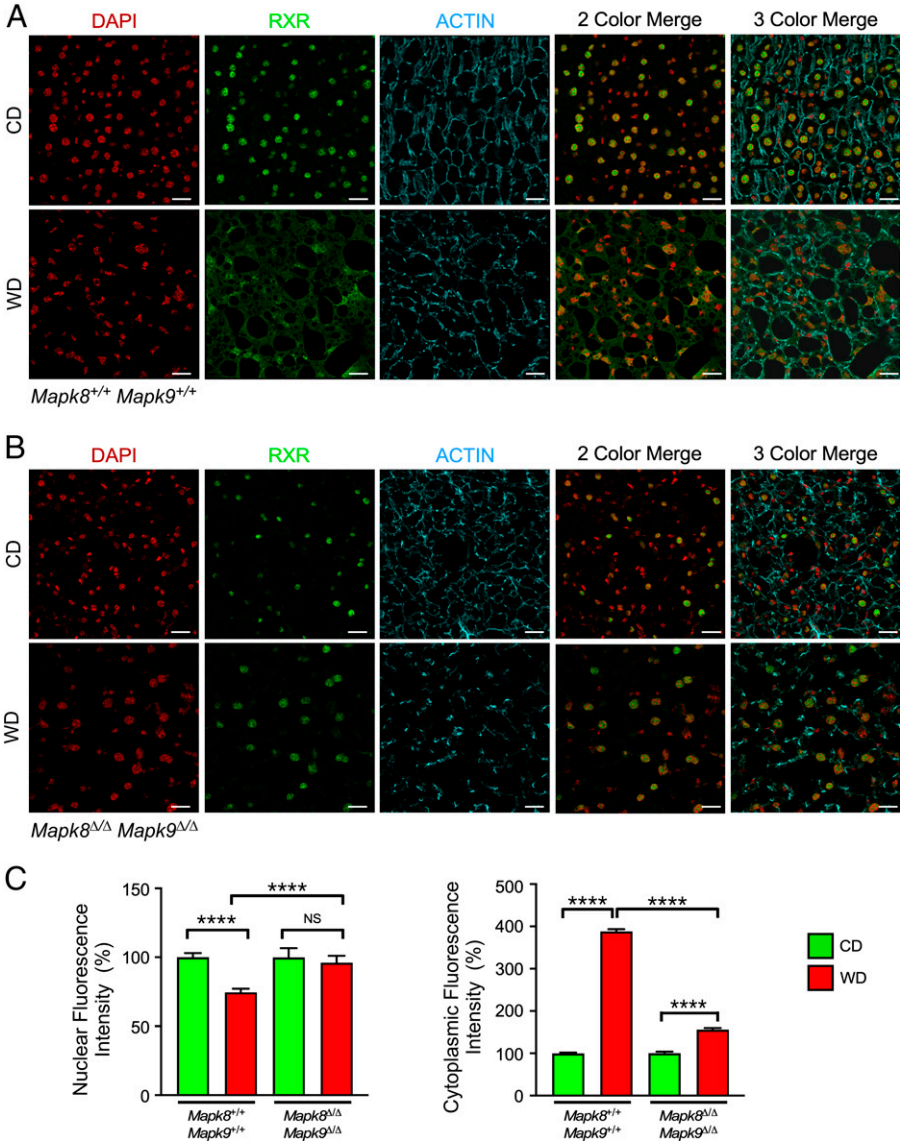

Fig. 4. Dietary stress causes JNK-dependent cytoplasmic accumulation of RXRα. (*A*) WT mice and (*B*) *Alb-Cre*$^{+/-}$ *Mapk8*$^{loxP/loxP}$ *Mapk9*$^{loxP/loxP}$ mice (age 8 wk) were fed a CD or a WD (16 wk). Liver sections were stained with an antibody to RXRα. DNA was stained with DAPI, and actin was stained with phalloidin. The sections were examined using a Leica SP8 confocal microscope. Representative images are presented. Scale bar, 20 μm. (*C*) The nuclear and cytoplasmic RXRα immunofluorescence was quantitated and presented as fluorescence intensity (mean ± SEM; ****$P < 0.0001$; not significant (NS), $P > 0.05$; n = 19–42 cells).

murine RXRα) were identified by studies using overexpression in COS-1 cells, but no changes in the transcriptional activity of RXRα complexes were detected (29). Subsequent studies using lower levels of overexpression in cultured mouse cells indicated that Ser^{22} phosphorylation may decrease the expression of a subset of RXRα target genes (46), although no changes in RXRα target gene expression were detected in a more recent study (47). Ser^{260} phosphorylation may inhibit the transcriptional activity of RXRα complexes (41, 48) by regulating the interaction of RXRα with corepressors/coactivators (35, 36). Phosphorylation on Ser^{260} may also inhibit the transcriptional activity of RXRα complexes by promoting ubiquitin-mediated degradation of RXRα in the cytoplasm (31), although other studies indicate that Ser^{260} phosphorylation may block ubiquitin-mediated degradation of RXRα (32, 33).

We identified Ser^{260} as a site of regulatory RXRα phosphorylation by JNK2α in the liver that suppresses expression of the hepatokine FGF21. We show that nutritional stress causes JNK-dependent relocalization of hepatic RXRα from the nucleus to the cytoplasm. This change in subcellular compartmentation provides a mechanism that can account for inhibition of *Fgf21* gene expression caused by JNK2α.

Signaling by JNK1 and JNK2. Studies of mice with hepatocyte-specific gene ablation demonstrate different functions of the JNK1 and JNK2 protein kinases (2, 3). The present study extends the understanding of isoform-specific signaling by identifying a key role of JNK2α in the regulation of hepatic RXRα/PPARα.

JNK alternatively spliced variants with the mutually exclusive exons 7a and 7b have been identified (26, 27). These alternative exons encode a segment of the substrate binding site on JNK (49). Inclusion of exon 7a in JNK1 and JNK2 mRNA leads to the expression of JNK with low JUN protein kinase activity (26). In contrast, inclusion of exon 7b in JNK1 and JNK2 leads to the expression of JNK with high JUN protein kinase activity (26). The difference in protein kinase activity between these isoforms reflects a difference in the affinity of substrate interaction (27). The major isoform in liver that includes exon 7b is JNK2 (also known as JNK2α) (26). Hepatic JNK2 deficiency eliminates the major JNK isoform with high levels of JUN protein kinase activity that include exon 7b (JNK2α). JNK2 deficiency therefore prevents JNK2α-mediated repression of RXRα/PPARα, but sustains activation of JNK1 isoforms. In contrast, JNK1 deficiency eliminates the expression of JNK1 isoforms with low levels of JUN protein kinase activity that include exon 7a and sustains the activation of JNK2 isoforms, including JNK2α, that subsequently represses RXRα/PPARα activity. This interpretation of the differential consequences of JNK1 and JNK2 deficiency predicts that the effect of JNK1 deficiency to decrease RXRα/PPARα activity should be eliminated by loss of JNK2 in a JNK1-deficient background. Indeed, compound deficiency of JNK1 plus JNK2 in hepatocytes causes a large increase in RXRα/PPARα activity (3) that is repressed by complementation with JNK2α (with exon 7b), but not by JNK2β (with exon 7a) (Fig. 1). These considerations indicate that the effects JNK1 and JNK2 deficiency reflect, at least in part, differential expression of alternatively spliced variants rather than intrinsic differences between JNK1 and JNK2.

Isoform-Specific Signaling by JNK. The mutually exclusive exons 7a and 7b encode a segment of the substrate binding site on JNK1 and JNK2 that determines substrate binding affinity (26, 27). Indeed, exon 7a-positive JNK1 and JNK2 exhibit low JUN protein kinase activity, while exon 7b-positive JNK1 and JNK2 exhibit high JUN protein kinase activity (26). However, it was unclear whether this difference between inclusion of exons 7a and 7b results in an activity change for all substrates or a change in substrate specificity. Our phosphoproteomics analysis suggests that the inclusion of exons 7a and 7b may direct JNK substrate specificity. Indeed, this analysis identifies a canonical JNK pathway (with exon 7b) that phosphorylates substrates that can activate AP1 transcriptional activity (e.g., JUN) and suppress nuclear hormone receptor signaling (RXRα) but also a noncanonical JNK pathway (with exon 7a) that phosphorylates alternative substrates, including ABCF1, CARD6, EIF4EBP2, GAS2, MTUS1, SRRM1, SRRM2, and PLEKHA6. The function of this noncanonical JNK signaling pathway is unclear and warrants further study.

Conclusions

This study establishes that splicoform-specific signaling by JNK causes inhibitory phosphorylation of RXRα. The mechanism of inhibition is mediated, in part, by relocalization of RXRα from the nucleus to the cytoplasm. Collectively, our analysis identifies a mechanism that mediates systemic insulin resistance caused by repression of FGF21 expression by the hepatic JNK signaling pathway.

Materials and Methods

Reagents, equipment, and software used in this study are described in *SI Appendix*, Table S1.

Animals. C57BL/6J mice (RRID: IMSR_JAX:000664), B6.Cg-*Speer6-ps1*$^{Tg(alb\text{-}cre)21Mgn}$/J mice (RRID: IMSR_JAX:003574) (50), and *Rxra*^{tm1Krc}/J mice (RRID: IMSR_JAX:013086) (51) were obtained from The Jackson Laboratory. *Alb*$^{tm1(cre/ERT2)Mtz}$ mice were provided by Daniel Metzger (30). We have previously described *Mapk8*$^{loxP/loxP}$ mice (52) and *Mapk9*$^{loxP/loxP}$ mice (53). The mice were backcrossed to the C57BL/6J strain (10 generations) and housed in a specific pathogen-free facility accredited by the Association for Assessment and Accreditation of Laboratory Animal Care (AAALAC) using laminar flow cages at 21 °C.

Mice (age 7 wk) were transduced with AAV8 vectors by tail vein injection. Mice (age 8 wk) were treated with tamoxifen (three intraperitoneal injections of 1 mg of tamoxifen dissolved in 100 μL of sunflower oil over 5 days). The mice were fed a CD (Purina, catalog number [Cat#] IsoPro 3000). At age 10 wk, the mice were maintained on a CD, fed a HFD (Bio-Serv, Cat# S3282) for 10 wk, or fed a WD (calories: 58% fat, 26% carbohydrate, and 16% protein [Research Diets, Cat# D17063001Bi], together with drinking water supplemented with 23.1 g/L fructose plus 18.9 g/L sucrose) for 24 wk. Blood glucose was measured with an Ascensia Breeze 2 glucometer (Bayer). Glucose tolerance tests (GTTs) and pyruvate tolerance tests (PTTs) were performed using methods described previously (54). FGF21 in plasma was measured by enzyme-linked immunosorbent assay (MilliporeSigma, Cat# EZRMFGF21-26K).

The studies were approved by the Institutional Animal Care and Use Committee of the University of Massachusetts Chan Medical School.

Genotype Analysis. Genomic DNA was genotyped using a PCR-based method. *Cre*$^{+}$ (450 bp) was detected using amplimers 5′-TTACTGACCGTACACCAAA TTTGCCTGC-3′ and 5′-CCTGGCAGCGATCGCTATTTTCCATGAGTG-3′. The amplimers 5′-CCTCAGGAAGAAAGGGCTTATTTC-3′ and 5′-GAACCACTGTTCCAATTTCCATCC-3′ detected the *Mapk8*$^{+}$ allele (1,550 bp), the *Mapk8*^{loxP} allele (1,095 bp), and the *Mapk8*$^{\Delta}$ allele (395 bp). The amplimers 5′-GTTTTGTAAAGGGAGCCGAC-3′ and 5′-CCTGACTACTGAGCCTGGTTTCT-3′ were used to detect the *Mapk9*$^{+}$ allele (224 bp) and the *Mapk9*^{loxP} allele (264 bp). The amplimers 5′-GGAATGTTTGGTCC TTTAG-3′, 5′-GCTATTCAGAGTTAAGTG-3′, and 5′-TTCATTCTAAGCTCAGACTC-3′ were used to detect the *Mapk9*^{loxP} allele (560 bp) and the *Mapk9*$^{\Delta}$ allele (400 bp). The amplimers 5′-CCATCCCTCAGGAAATATGG-3′ and 5′-AGAGGATGGGTGAACTTAA TGACA-3′ were used to detect the *Rxra*$^{+}$ allele (613 bp) and the *Rxra*^{loxP} allele (700 bp). The amplimers were obtained from Eurofins Genomics.

AAV8 Transduction Studies. The LacZ expression vector pAAV-CB6-PI-LacZ has been described (55). Wild-type mouse JNK2α2 and JNK2β2 *Bam*H1/*Eco*RI fragments (26) were cloned by blunt-end ligation into the *Eco*RI site of the pAAV-CB6-PI vector (55) following treatment with a Klenow fragment (New England Biolabs, Cat# M021S). The human *Rxrα* complementary DNA in the plasmid pCV-Sport-RxRα (Addgene plasmid 8882, RRID: Addgene_8882) (56) was mutated to replace phosphorylation site codons with the QuikChange II kit (Agilent, Cat# 200521) and subcloned as *Eco*RI fragments into the *Eco*RI site of pAAV-CB6-PI. High-titer recombinant AAV8 were produced in the University of Massachusetts Gene Therapy Vector Core. Mice were injected intravenously with 3.0×10^{11} genome copies of AAV8 vector per mouse.

Analysis of Liver Sections. Mice were euthanized and liver fragments were frozen in optimal cutting temperature compound (Thermo Fisher Scientific, Cat# 23-730-571; Waltham, MA). Frozen sections (7 μm) were prepared and fixed with 4% paraformaldehyde (Thermo Fisher Scientific, Cat# 50-980-487) in phosphate-buffered saline (PBS) at 4 °C. The sections were stained with 1:100 RXRα antibody (Abcam, Cat# ab125001, RRID: AB_10975632) and detected using Alexa Fluor 633-conjugated goat anti-rabbit immunoglobulin G (heavy & light chain) antibody (Thermo Fisher Scientific, Cat# A-11034, RRID: AB_2576217) at 4 °C. Actin was stained with 1:200 Alexa Fluor 546-conjugated phalloidin (Thermo Fisher Scientific, Cat# A22283). DNA was detected by staining with DAPI (Thermo Fisher Scientific, Cat# D3571, RRID: AB_2307445). Fluorescence was visualized using a Leica TCS SP8 confocal microscope. The fluorescence was quantitated from grayscale images using ImageJ2 software. Regions of interest were created that encompassed nuclei or cytoplasmic areas. Fluorescence was expressed as the average value within the region of interest (sum of all gray values of all pixels in the selected area divided by the number of pixels) and was normalized to control diet for each genotype.

Mass Spectroscopy. The livers of two control mice, two hepatocyte-specific JNK1/2 knockout mice, two hepatocyte-specific JNK1/2 knockout mice complemented with JNK2α, and two hepatocyte-specific JNK1/2 knockout mice complemented with JNK2β were examined by a multiplexed tandem mass tags-based procedure using mass spectroscopy. The mice were euthanized individually and their livers were harvested, washed twice with PBS, and snap frozen in liquid nitrogen. The livers were mechanically lysed with an Omni mixer homogenizer in sodium dodecy sulfate lysis buffer: 2% SDS (wt/vol), 50 mM HEPES (pH 7.2), 150 mM NaCl, 10 mM N-ethylmaleimide, 1x protease inhibitor mixture (Roche), and 1x PhosSTOP phosphatase inhibitor mixture (Roche). Suspensions were centrifuged at maximum speed for 15 min at 4 °C, and lysates were transferred to a clean 50-mL tubes. Lysates were reduced for 1 h at room temperature with 5 mM Tris(2-carboxyethyl)phosphine hydrochloride, followed by cysteine alkylation with iodoacetamide via a 30-min incubation at room temperature in the dark. Protein content was extracted twice by methanol-chloroform precipitation and subsequent ice-cold acetone washes. Protein pellets were resuspended in 8 M urea with 50 mM HEPES (pH 8.5) buffer, and protein concentrations were measured by bicinchoninic acid assay (Thermo Fisher Scientific). Then, 10 mg of protein per sample were diluted to 4 M urea with 50 mM HEPES (pH 8.5) and digested at 30 °C for 6 h with endoproteinase Lys-C (Wako, Japan) at a 1:100 enzyme/protein ratio. The mixtures were then diluted to 1 M urea with 50 mM HEPES (pH 8.5), and trypsin was added at a 1:50 enzyme/protein ratio. The reaction was incubated overnight at 37 °C with gentle end-over-end rotation and stopped by acidification with formic acid (FA) 0.5% (vol/vol) (∼pH 2). Peptides were subjected to tC18 Sep-Pak solid-phase extraction (SPE) cartridges (Waters) and lyophilized. Peptides were resuspended in 100 mM HEPES (pH 8.5), and peptide concentration was determined using the microBCA assay (Thermo Fisher Scientific). From each sample, 50 μg of peptide was removed for protein-level analysis and the remaining amount of the liver digests was used for phosphoprotein enrichment.

Phosphopeptides were enriched using a method based on that of Kettenbach and Gerber (57). In brief, Titanosphere TiO_2 5-μm particles (GL Biosciences, Tokyo, Japan) were washed three times with 2 M lactic acid/50% acetonitrile. Peptides were resuspended in 2.5 mL of 2 M lactic acid/50% acetonitrile. For ∼10 mg of peptide digest, 40-mg beads were added and incubated with gentle rotation for 1 h at room temperature. Beads were washed twice with 2.5 mL of 2 M lactic acid/50% acetonitrile, then twice with 2.5 mL of 50% acetonitrile/0.1% trifluoroacetic acid, and finally twice with 2.5 mL of 25% acetonitrile/0.1% TFA. Enriched phosphopeptides were eluted twice with 500 μL of 50 mM K_2HPO_4 (pH 10) and vacuum centrifuged to dryness.

In preparation for TMT labeling, desalted peptides (both for 50-μg protein-level and 10-mg phosphopeptide-level analysis) were dissolved in 200 mM HEPES (pH 8.5). Peptides from each sample were labeled with a specific TMT reagent, and channels 130c and 131 were duplicate mixtures from peptides of each of the eight individual samples. TMT reagents (0.8 mg) were dissolved in anhydrous acetonitrile (40 μL), of which 10 μL was added to the peptides (resuspended in 70 μL of 100 mM HEPES, pH 8.5), along with 20 μL of acetonitrile, to achieve a final acetonitrile concentration of 30% (vol/vol). Following incubation at room temperature for 1 h, the reaction was quenched with hydroxylamine to a final concentration of 0.3% (vol/vol). The TMT-labeled samples were combined at a 1:1:1:1:1:1:1:1:1:1 ratio. The sample was vacuum centrifuged to near dryness and subjected to C18 SPE (Sep-Pak, Waters).

Protein-level and total phosphoproteome analysis was performed using TMT-labeled peptides subjected to orthogonal basic-pH reverse-phase fractionation. Peptides were solubilized in 5% acetonitrile with 10 mM ammonium bicarbonate (pH 8) buffer and separated on an Agilent 300 Extend C18 column (5-μm particles, 4.6-mm inner diameter [ID], and 220 mm in length). Using an Agilent 1100 binary pump equipped with a degasser and a photodiode array detector (set at 220- and 280-nm wavelengths) from Thermo Fisher Scientific, a 50-min linear gradient from 5 to 35% acetonitrile in 10 mM ammonium bicarbonate (pH 8) at a flow rate of 0.8 mL/min with an Agilent 300 Extend C18 column (5-μm particles, 4.6-mm ID, and 220 mm in length) separated the peptide mixture into a total of 96 fractions. The 96 fractions were consolidated into 24 samples in a checkerboard manner, acidified with 1% FA, and vacuum centrifuged to dryness. Each fraction was desalted via StageTip, dried via vacuum centrifugation, and reconstituted in 5% acetonitrile and 5% FA for liquid chromatography–mass spectrometry processing.

All spectra were acquired on an Orbitrap Fusion (Thermo Fisher Scientific) coupled to an Easy-nLC 1000 (Thermo Fisher Scientific) ultra–high-pressure liquid chromatography pump. Peptides were separated on an in-house–packed 100 μm ID column containing 0.5 cm of Magic C4 resin (5 μm, 100 Å; Michrom Bioresources), serving as a frit, followed by 25 cm of Sepax Technologies GP-C18 resin (1.8 μm, 120 Å; Newark, DE) using a 2-h gradient of 3 to 22% ACN and 0.125% FA for ∼300 nL/min. For each analysis, we loaded ∼1 μg onto the column. The instrument was operated in the data-dependent mode, and each analysis used a 2nd generation product ion spectra (MS^3)-based tandem mass tag method (58, 59). The scan sequence began with a precursor intensity mass spectrum (MS^1) (Orbitrap analysis: resolution of 120,000, automatic gain control [AGC] target of 2×10^5, and maximum injection time of 100 ms). The 10 most intense ions were selected for first generation product ion spectra (MS^2) analysis. Precursor ions were filtered according charge state ($z > 1$), monoisotopic peak assignment, and a dynamic window of 75 s ± 10 ppm. MS^2 precursors were isolated with a quadrupole mass filter set to a width of 0.5 *m/z*. Following acquisition of each MS^2 spectrum, we collected an MS^3 spectrum using our recently described method in which multiple MS^2 fragment ions are captured in the MS^3 precursor population using isolation waveforms with multiple frequency notches (58). MS^3 precursors were fragmented by higher energy C-trap dissociation and analyzed using the Orbitrap (normalized collision energy of 55%, maximum AGC of 5×10^4, maximum injection time of 250 ms, isolation specificity of 0.5 Th, and resolution of 60,000 at 400 Th).

Mass spectra were processed using a Sequest-based in-house software pipeline. MS spectra were converted to mzXML using a modified version of ReAdW.exe. Database searching included all entries from the mouse Uniprot database (August 10, 2011), which was concatenated with a reverse database composed of all protein sequences in reversed order. Searches were performed using a 50-ppm precursor ion tolerance. TMT tags on lysine residues and peptide N termini (+229.162932 Da) and carbamidomethylation of cysteine residues (+57.02146 Da) were set as static modifications, while oxidation of methionine residues (+15.99492 Da) was set as a variable modification. For phosphoprotein analysis, +79.96633 Da on serine, threonine, and tyrosine was also set as a variable modification.

Peptide spectral matches (PSMs) were altered to a 1% false discovery rate (60). PSM filtering was performed using a linear discriminant analysis, as described previously (61), while considering the following parameters: XCorr,

ΔCn, missed cleavages, peptide length, charge state, and precursor mass accuracy. For TMT-based reporter ion quantitation, we extracted the signal-to-noise ratio for each TMT channel and found the closest-matching centroid to the expected mass of the TMT reporter ion.

The search space for each reporter ion was limited to a range of 0.002 Th to prevent overlap between the isobaric reporter ions. For protein-level comparisons, PSMs were identified, quantified, and collapsed to a 1% FDR and then further collapsed to a final protein-level FDR of 1%. Furthermore, protein assembly was guided by principles of parsimony to produce the smallest set of proteins necessary to account for all observed peptides. We used a modified version of the Ascore algorithm to quantify the confidence with which each phosphorylation site could be assigned to a particular residue. Phosphorylation sites with Ascore >13 ($P \leq 0.05$) were considered confidently localized to a particular residue (61).

Proteins and phosphorylation sites were quantified by summing reporter ion counts across all matching PSMs using in-house software, as described previously (61). Briefly, a 0.003-Th window around the theoretical *m/z* of each reporter ion (126, 127N, 127C, 128N, 128C, 129N, 129C, 130N, 130C, and 131) was scanned for ions, and the maximum intensity nearest the theoretical *m/z* was used. For each peptide, a total minimum sum signal-to-noise value of 200 and an isolation purity greater than 70% was required. Protein quantitation values were exported for further analysis using Excel, MATLAB, or Mathematica.

The complex heatmap package (version 1.10.2) (62) was used to display differences in hepatic protein phosphorylation. The clustering_distance_rows parameter was set to maximum; the clustering_method_rows parameter was set to ward.D. Phosphorylation sites were included that conformed to pSer-Pro or pThr-Pro motifs and were differentially expressed (>1.2) between control (*Alb-Cre*$^{+/-}$ *Mapk8*$^{+/+}$ *Mapk9*$^{+/+}$) and JNK-deficient (*Alb-Cre*$^{+/-}$ *Mapk8*$^{loxP/loxP}$ *Mapk9*$^{loxP/loxP}$) mice. Phosphorylation sites were excluded if differential phosphorylation in the JNK-deficient mice was not partially suppressed (>1.2) by JNK2 expression. The remaining phosphorylation sites were examined by heatmap analysis of the mean phosphorylation (k = 2).

The mass spectrometry data have been deposited to the ProteomeXchange Consortium (http://proteomecentral.proteomexchange.org) (63) via the Proteomics Identification Database (PRIDE) partner repository (accession no. PXD034183) (64).

Primary Hepatocytes. Primary hepatocytes were isolated from mice using a modified two-step perfusion method (65) using liver perfusion media (Thermo Fisher Scientific, Cat# 17701038) and liver digest buffer (Thermo Fisher Scientific, Cat# 17703034). Cells were seeded on plates (precoated [1 h] rat tail collagen I; Thermo Fisher Scientific, Cat# A1048301) in Dulbecco's Modified Eagle's Medium plus 10% fetal bovine serum, 2 mM sodium pyruvate, 1 μM dexamethasone, and 100 nM insulin plus 2% penicillin/streptomycin. After attachment (2 h), the medium was removed and the hepatocytes were incubated (22 h) in maintenance medium (DMEM [4.5 g/L glucose] supplemented with 10% FBS, 0.2% bovine serum albumin, 2 mM sodium pyruvate, 2% penicillin/streptomycin, 0.1 μM dexamethasone, and 1 nM insulin). The hepatocytes were incubated (16 h) with the PPARα agonist (100 μM) fenofibrate (MilliporeSigma, Cat# 6020) or solvent control (dimethyl sulfoxide).

RNA Analysis. The expression of mRNA was examined by qPCR analysis using a Quantstudio PCR machine (Thermo Fisher Scientific) and a TaqMan probe for *Pdk4* (Mm01166878_m1) (Thermo Fisher Scientific). Human *Rxra* mRNA was detected using the probe Hs01067640_m1 (Thermo Fisher Scientific). Mouse *Rxra* mRNA was detected using Universal ProbeLibrary Probe 63 (Roche, Cat# 04688619001) and amplimers 5′-CAGTACTGCCGCTACCAGAA-3′ and 5′-CGTTCTCATTCCGGTCCTT-3′ (Eurofins Genomics). The relative mRNA expression was normalized by measurement of the amount of 18S RNA in each sample.

Immunoblot Analysis. Extracts (20 to 50 μg of protein) were examined by protein immunoblot analysis by probing with antibodies to JUN (Cell Signaling Technology, Cat# 2315, RRID: AB_490780), pSer^{63}-JUN (Cell Signaling Technology, Cat# 9261, RRID: AB_213016292), GAPDH (Santa Cruz Biotechnology, Cat# sc-25778, RRID: AB_10167668), JNK1/2 (BD Biosciences, Cat# 554285, RRID: AB_395344), FLAG (M2) (MilliporeSigma, Cat# P2983, RRID: AB_439685), RXRα (Abcam, Cat# ab125001, RRID: AB_10975632), pSer^{22} mouse RXRα (affinity-purified rabbit polyclonal antibody made to keyhole limpet hemocyanine conjugated to Cys-QVNSSSLNpSPTGR), and α-tubulin (MilliporeSigma, clone B-5-1-2, Cat# T5168, RRID: _477579). IRDye 680RD-conjugated goat anti-mouse IgG antibody (LI-COR Biosciences, Cat# 926-68070, RRID: AB_10956588) and IRDye 800CW-conjugated goat anti-rabbit IgG (LI-COR Biosciences, Cat# 926-32211, RRID: AB_621843) were used to detect immune complexes with the Odyssey infrared imaging system (LI-COR Biosciences).

Statistical Analysis. Data are presented as the mean and SE. Statistical analysis was performed using GraphPad Prism version 7 (GraphPad Software). ANOVA with Bonferroni's test was used to determine significance with an assumed confidence interval of 95%. Two-tailed, unpaired *t* test with Welch's correction was used for pairwise comparisons. Statistical significance was defined as $P < 0.05$.

Data, Materials, and Software Availability. Sources for materials used in this study are described in *Materials and Methods* and *SI Appendix*, Table S1. Data are presented in *SI Appendix*, Dataset S1. The mass spectrometry proteomics data have been deposited to the ProteomeXchange Consortium via the PRIDE (63) partner repository with the dataset identifier PXD034183 (64). All other study data are included in the article and/or supporting information.

ACKNOWLEDGMENTS. We thank Kathy Gemme for expert administrative assistance and Drs. Daniel Metzger and Pierre Chambon for providing *Alb*$^{tm1(cre/ERT2)Mtz}$ mice. These studies were supported by American Heart Association grant 19CDA34660270 (to M.S.H.), NIH grant R01 DK107220 (to R.J.D.), and the Medical Research Council (to S.V.).

Author affiliations: [a]Medical Research Council, London Institute of Medical Sciences, Du Cane Road, London W12 0NN, United Kingdom; [b]Institute of Clinical Sciences, Imperial College London, Hammersmith Hospital Campus, Du Cane Road, London W12 0NN, United Kingdom; [c]Program in Molecular Medicine, Chan Medical School, University of Massachusetts, Worcester, MA 01605; [d]Department of Cell Biology, Harvard Medical School, Harvard University, Boston, MA 01451; and [e]Horae Gene Therapy Center, Chan Medical School, University of Massachusetts, Worcester, MA 01605

1. G. Sabio, R. J. Davis, cJun NH2-terminal kinase 1 (JNK1): Roles in metabolic regulation of insulin resistance. *Trends Biochem. Sci.* **35**, 490–496 (2010).
2. G. Sabio *et al.*, Prevention of steatosis by hepatic JNK1. *Cell Metab.* **10**, 491–498 (2009).
3. S. Vernia *et al.*, The PPARα-FGF21 hormone axis contributes to metabolic regulation by the hepatic JNK signaling pathway. *Cell Metab.* **20**, 512–525 (2014).
4. M. K. Badman *et al.*, Hepatic fibroblast growth factor 21 is regulated by PPARalpha and is a key mediator of hepatic lipid metabolism in ketotic states. *Cell Metab.* **5**, 426–437 (2007).
5. T. Inagaki *et al.*, Endocrine regulation of the fasting response by PPARalpha-mediated induction of fibroblast growth factor 21. *Cell Metab.* **5**, 415–425 (2007).
6. S. Vernia, J. Cavanagh-Kyros, T. Barrett, C. Tournier, R. J. Davis, Fibroblast growth factor 21 mediates glycemic regulation by hepatic JNK. *Cell Rep.* **14**, 2273–2280 (2016).
7. F. M. Fisher, E. Maratos-Flier, Understanding the physiology of FGF21. *Annu. Rev. Physiol.* **78**, 223–241 (2016).
8. S. A. Kliewer, D. J. Mangelsdorf, A dozen years of discovery: Insights into the physiology and pharmacology of FGF21. *Cell Metab.* **29**, 246–253 (2019).
9. L. D. BonDurant, M. J. Potthoff, Fibroblast growth factor 21: A versatile regulator of metabolic homeostasis. *Annu. Rev. Nutr.* **38**, 173–196 (2018).
10. K. H. Flippo, M. J. Potthoff, Metabolic messengers: FGF21. *Nat. Metab.* **3**, 309–317 (2021).
11. F. M. Fisher *et al.*, FGF21 regulates PGC-1α and browning of white adipose tissues in adaptive thermogenesis. *Genes Dev.* **26**, 271–281 (2012).
12. P. A. Dutchak *et al.*, Fibroblast growth factor-21 regulates PPARγ activity and the antidiabetic actions of thiazolidinediones. *Cell* **148**, 556–567 (2012).
13. Z. Huang *et al.*, The FGF21-CCL11 axis mediates Beiging of white adipose tissues by coupling sympathetic nervous system to type 2 immunity. *Cell Metab.* **26**, 493–508.e4 (2017).
14. W. L. Holland *et al.*, An FGF21-adiponectin-ceramide axis controls energy expenditure and insulin action in mice. *Cell Metab.* **17**, 790–797 (2013).
15. Z. Lin *et al.*, Adiponectin mediates the metabolic effects of FGF21 on glucose homeostasis and insulin sensitivity in mice. *Cell Metab.* **17**, 779–789 (2013).
16. M. S. Han *et al.*, A feed-forward regulatory loop in adipose tissue promotes signaling by the hepatokine FGF21. *Genes Dev.* **35**, 133–146 (2021).
17. A. L. Bookout *et al.*, FGF21 regulates metabolism and circadian behavior by acting on the nervous system. *Nat. Med.* **19**, 1147–1152 (2013).
18. B. M. Owen *et al.*, FGF21 acts centrally to induce sympathetic nerve activity, energy expenditure, and weight loss. *Cell Metab.* **20**, 670–677 (2014).
19. S. Talukdar *et al.*, FGF21 regulates sweet and alcohol preference. *Cell Metab.* **23**, 344–349 (2016).
20. G. Schumann *et al.*, KLB is associated with alcohol drinking, and its gene product β-Klotho is necessary for FGF21 regulation of alcohol preference. *Proc. Natl. Acad. Sci. U.S.A.* **113**, 14372–14377 (2016).
21. S. Søberg *et al.*, FGF21 is a sugar-induced hormone associated with sweet intake and preference in humans. *Cell Metab.* **25**, 1045–1053.e6 (2017).
22. S. von Holstein-Rathlou *et al.*, FGF21 mediates endocrine control of simple sugar intake and sweet taste preference by the liver. *Cell Metab.* **23**, 335–343 (2016).
23. P. Song *et al.*, The hormone FGF21 stimulates water drinking in response to ketogenic diet and alcohol. *Cell Metab.* **27**, 1338–1347.e4 (2018).

24. N. Douris *et al.*, Central fibroblast growth factor 21 browns white fat via sympathetic action in male mice. *Endocrinology* **156**, 2470–2481 (2015).
25. R. M. Evans, D. J. Mangelsdorf, Nuclear receptors, RXR, and the Big Bang. *Cell* **157**, 255–266 (2014).
26. S. Vernia *et al.*, An alternative splicing program promotes adipose tissue thermogenesis. *eLife* **5**, e17672 (2016).
27. S. Gupta *et al.*, Selective interaction of JNK protein kinase isoforms with transcription factors. *EMBO J.* **15**, 2760–2770 (1996).
28. R. J. Davis, Signal transduction by the JNK group of MAP kinases. *Cell* **103**, 239–252 (2000).
29. S. Adam-Stitah, L. Penna, P. Chambon, C. Rochette-Egly, Hyperphosphorylation of the retinoid X receptor alpha by activated c-Jun NH2-terminal kinases. *J. Biol. Chem.* **274**, 18932–18941 (1999).
30. M. Schuler, A. Dierich, P. Chambon, D. Metzger, Efficient temporally controlled targeted somatic mutagenesis in hepatocytes of the mouse. *Genesis* **39**, 167–172 (2004).
31. T. L. Zimmerman, S. Thevananther, R. Ghose, A. R. Burns, S. J. Karpen, Nuclear export of retinoid X receptor alpha in response to interleukin-1beta-mediated cell signaling: Roles for JNK and SER260. *J. Biol. Chem.* **281**, 15434–15440 (2006).
32. S. Adachi *et al.*, Phosphorylation of retinoid X receptor suppresses its ubiquitination in human hepatocellular carcinoma. *Hepatology* **35**, 332–340 (2002).
33. R. Matsushima-Nishiwaki *et al.*, Phosphorylation of retinoid X receptor alpha at serine 260 impairs its metabolism and function in human hepatocellular carcinoma. *Cancer Res.* **61**, 7675–7682 (2001).
34. K. Yoshimura *et al.*, Phosphorylated retinoid X receptor alpha loses its heterodimeric activity with retinoic acid receptor beta. *Cancer Sci.* **98**, 1868–1874 (2007).
35. M. Macoritto *et al.*, Phosphorylation of the human retinoid X receptor alpha at serine 260 impairs coactivator(s) recruitment and induces hormone resistance to multiple ligands. *J. Biol. Chem.* **283**, 4943–4956 (2008).
36. Z. Zhang *et al.*, Constitutive activation of the mitogen-activated protein kinase pathway impairs vitamin D signaling in human prostate epithelial cells. *J. Cell. Physiol.* **224**, 433–442 (2010).
37. X. Cao *et al.*, Retinoid X receptor regulates Nur77/TR3-dependent apoptosis [corrected] by modulating its nuclear export and mitochondrial targeting. *Mol. Cell. Biol.* **24**, 9705–9725 (2004).
38. K. Prüfer, J. Barsony, Retinoid X receptor dominates the nuclear import and export of the unliganded vitamin D receptor. *Mol. Endocrinol.* **16**, 1738–1751 (2002).
39. Y. Zhao *et al.*, Casein kinase 1alpha interacts with retinoid X receptor and interferes with agonist-induced apoptosis. *J. Biol. Chem.* **279**, 30844–30849 (2004).
40. H. Y. Lee *et al.*, Stress pathway activation induces phosphorylation of retinoid X receptor. *J. Biol. Chem.* **275**, 32193–32199 (2000).
41. C. Solomon, J. H. White, R. Kremer, Mitogen-activated protein kinase inhibits 1,25-dihydroxyvitamin D3-dependent signal transduction by phosphorylating human retinoid X receptor alpha. *J. Clin. Invest.* **103**, 1729–1735 (1999).
42. S. Zhang *et al.*, The roles of GSK-3β in regulation of retinoid signaling and sorafenib treatment response in hepatocellular carcinoma. *Theranostics* **10**, 1230–1244 (2020).
43. J. Liang *et al.*, miR-27a-3p targeting RXRα promotes colorectal cancer progression by activating Wnt/β-catenin pathway. *Oncotarget* **8**, 82991–83008 (2017).
44. J. Tang *et al.*, LncRNA DANCR upregulates PI3K/AKT signaling through activating serine phosphorylation of RXRA. *Cell Death Dis.* **9**, 1167 (2018).
45. K. Sun *et al.*, Phosphorylation of a conserved serine in the deoxyribonucleic acid binding domain of nuclear receptors alters intracellular localization. *Mol. Endocrinol.* **21**, 1297–1311 (2007).
46. J. Bastien, S. Adam-Stitah, J. L. Plassat, P. Chambon, C. Rochette-Egly, The phosphorylation site located in the A region of retinoic X receptor alpha is required for the antiproliferative effect of retinoic acid (RA) and the activation of RA target genes in F9 cells. *J. Biol. Chem.* **277**, 28683–28689 (2002).
47. J. Ardenkjaer-Larsen *et al.*, Insulin-induced serine 22 phosphorylation of retinoid X receptor alpha is dispensable for adipogenesis in brown adipocytes. *Adipocyte* **9**, 142–152 (2020).
48. N. Bruck *et al.*, Phosphorylation of the retinoid x receptor at the omega loop, modulates the expression of retinoic-acid-target genes with a promoter context specificity. *Cell. Signal.* **17**, 1229–1239 (2005).
49. H. Enslen, R. J. Davis, Regulation of MAP kinases by docking domains. *Biol. Cell* **93**, 5–14 (2001).
50. C. Postic *et al.*, Dual roles for glucokinase in glucose homeostasis as determined by liver and pancreatic beta cell-specific gene knock-outs using Cre recombinase. *J. Biol. Chem.* **274**, 305–315 (1999).
51. J. Chen, S. W. Kubalak, K. R. Chien, Ventricular muscle-restricted targeting of the RXRalpha gene reveals a non-cell-autonomous requirement in cardiac chamber morphogenesis. *Development* **125**, 1943–1949 (1998).
52. M. Das *et al.*, Suppression of p53-dependent senescence by the JNK signal transduction pathway. *Proc. Natl. Acad. Sci. U.S.A.* **104**, 15759–15764 (2007).
53. M. S. Han *et al.*, JNK expression by macrophages promotes obesity-induced insulin resistance and inflammation. *Science* **339**, 218–222 (2013).
54. G. Sabio *et al.*, A stress signaling pathway in adipose tissue regulates hepatic insulin resistance. *Science* **322**, 1539–1543 (2008).
55. A. Rashnonejad, G. A. Chermahini, S. Li, F. Ozkinay, G. Gao, Large-scale production of adeno-associated viral vector serotype-9 carrying the human survival motor neuron gene. *Mol. Biotechnol.* **58**, 30–36 (2016).
56. P. Tontonoz, E. Hu, R. A. Graves, A. I. Budavari, B. M. Spiegelman, mPPAR gamma 2: Tissue-specific regulator of an adipocyte enhancer. *Genes Dev.* **8**, 1224–1234 (1994).
57. A. N. Kettenbach, S. A. Gerber, Rapid and reproducible single-stage phosphopeptide enrichment of complex peptide mixtures: Application to general and phosphotyrosine-specific phosphoproteomics experiments. *Anal. Chem.* **83**, 7635–7644 (2011).
58. G. C. McAlister *et al.*, MultiNotch MS3 enables accurate, sensitive, and multiplexed detection of differential expression across cancer cell line proteomes. *Anal. Chem.* **86**, 7150–7158 (2014).
59. L. Ting, R. Rad, S. P. Gygi, W. Haas, MS3 eliminates ratio distortion in isobaric multiplexed quantitative proteomics. *Nat. Methods* **8**, 937–940 (2011).
60. J. E. Elias, S. P. Gygi, Target-decoy search strategy for increased confidence in large-scale protein identifications by mass spectrometry. *Nat. Methods* **4**, 207–214 (2007).
61. E. L. Huttlin *et al.*, A tissue-specific atlas of mouse protein phosphorylation and expression. *Cell* **143**, 1174–1189 (2010).
62. Z. Gu, R. Eils, M. Schlesner, Complex heatmaps reveal patterns and correlations in multidimensional genomic data. *Bioinformatics* **32**, 2847–2849 (2016).
63. Y. Perez-Riverol *et al.*, The PRIDE database resources in 2022: a hub for mass spectrometry-based proteomics evidences. *Nucleic Acids Res.* **50**, D543–D552 (2022).
64. S. Vernia *et al.*, Phosphorylation of RXRα mediates the effect of JNK to suppress hepatic FGF21 expression and promote metabolic syndrome. ProteomeXchange Consortium. http://www.ebi.ac.uk/pride/archive/projects/PXD034183. Deposited 29 May 2022.
65. P. O. Seglen, Preparation of isolated rat liver cells. *Methods Cell Biol.* **13**, 29–83 (1976).